Proceedings of the ASME 2012 International Design Engineering Technical Conferences & Computers and Information in Engineering Conference
IDETC/CIE 2012
August 12-15, 2012, Chicago, IL, USA

DETC2012-70292

Bipedal Walking Robot Driven by Elastic Cables

Elvedin Kljuno and **Robert L. Williams II**
Mechanical Engineering Department, Ohio University
Athens, Ohio 45701
E-mail: williar4@ohio.edu

Jim Zhu
Electrical Engineering Department, Ohio University, Athens, Ohio 45701
E-mail: zhuj@ohio.edu

ABSTRACT

This paper presents a design concept and analysis of a bipedal walking robot with a novel type of actuation using elastic cables. Each leg has 6-dof, the trunk has 3-dof, and each arm has 1-shoulder-dof. Conventional walking robots consist of joint-attached drives at revolute joints. This yields relatively heavy legs and arms with high moments of inertia, which makes balancing robot dynamic walking difficult due to the high inertial forces of distal segments.

The cable-based actuation system is designed for the most kinetically-active biped segments, such as lower legs. These consist of DC motors located on the trunk, elastic cables (with serially-connected springs) and cable routing with specially-designed pulleys. Since the trunk segment accelerations are significantly lower than the leg segments accelerations, it is expected that the overall energy required by the cable-actuated robot is significantly lower than the energy input to a directly-actuated biped.

Another novelty in the biped actuation system design is the use of elastic rather than non-elastic cables, for two reasons: smoothing out the sharp impulses due to the foot-ground collision and reduction of the number of motors to actuate each joint. Non-elastic cable-based drives require each cable to be pulled by a separate motor, which would double the number of motors and increase the weight. This problem can be solved using elastic cables and specially-shaped pulleys to reduce the number of motors with a slight increase in controller complexity.

The bipedal walking robot architecture with cable drives mimics the human body architecture, where the hip joint is a 3-dof spherical joint, 1-dof knee joint, and 2-dof ankle joint. The architecture is more compact compared to the conventional joint attached drive architecture, wherein all revolute joints are separated.

Based on the kinematic and dynamic analysis of the robot, a controller is designed and the perturbation robustness tested. A feedback linearization controller design is used, requiring system dynamics knowledge. Steps toward hardware implementation have been made, since we have implemented an elastic cable actuation system on a robotic cat prior to the concept design for the bipedal robot. The difficulties are discussed, including future plans for improvements and hardware testing.

1. INTRODUCTION

Simplicity in design and implementation is one of the most important reasons that robotic manipulators are mainly actuated by joint directly mounted rotary motors, the joint attached drives. The rotation of the motor shaft is proportionally mapped into rotation of connected robotic links about the joint axis, using a gear set. Design methodology and the theoretical treatment of robotic manipulator systems penetrated into a relatively new robotic field, the robotic walkers. While joint mounted motors are suitable for relatively slowly moving robotic manipulators/systems with a stationary support base, they are unlikely to met needs of the robotic walkers. Although there exist examples of successful and advanced robotic walkers with directly joint mounted motors [1,2], they necessarily consume higher amounts of energy comparing to their corresponding biological walkers [3].

However, biological walkers that use an inverted pendulum like mechanism [4,5,6] are considered energy efficient relatively with respect to the state of the art robotic walkers [7,8], using a different kind of actuators, the muscles, which can be considered as elastic (stretchable) linear actuators. Energy efficiency and the level of the walk cycle precision and smoothness are among important reasons for mimicking biological walkers. As the fundamental actuator unit, the muscle

behavior and structure attract special attention of research in robotics. There have been a number of attempts to produce artificial muscles for use in robotics [9-12], based on different principles such as pneumatics, piezoelectric effect, magnetostriction, etc.

One of the possibilities of a walking robot muscle-like actuation is to use (elastic) cables. Applications of the cable actuation in general robotics [13] show that the main feature, among other interesting features, of the cable actuation is the possibility to achieve relatively high accelerations, due to the reduced mass of the most kinetically-active segments of the robots.

Since the walking robots usually have to carry an independent energy source (batteries), it is the most critical to reduce the energy consumed per distance walked. Using the cables the motors are moved to the sections of the robot that are the least kinetically-active and experience the lowest accelerations. The main benefits are: the balancing stability of the robot is improved and the energy consumption is reduced due to the reduced mass of the fast moving segments of the walking robot. It will also lead to significantly reduced overall weight of the robot.

Further benefit of using cables is obtained by introducing elastic cables in the cable driven robot design. Foot-ground collisions generate impulsive forces and torques through the joints. Using elastic cables, the shock energy is absorbed while the motor torques are smoothened. The joint angular velocities remain continuous through out the entire walking cycle, which allows us to avoid using the continuous and the collision dynamics combination (the hybrid dynamics).

Some work has been done in the area of cable actuation in the walking robotics. A partially cable actuated hexapod is analyzed in [14]. A quadruped walking robot with knee joints driven via elastic cables [15] has been designed with some success in terms of reducing energy input and smoothness of the walk. However, there is no evidence that a bipedal walking robot with elastic cables based actuators has been designed/built or such a design discussed. Therefore, this paper introduces a novelty concept that certainly has significant benefits that will be emphasized throughout the test results analysis.

2. ELASTIC CABLE ACTUATED BIPEDAL WALKING ROBOT ARCHITECTURE

Besides the benefits of reducing the energy consumed per walked distance and reducing the mass, and consequently the inertial forces, of the most kinetically active segments (lower legs, feet), another very important benefit of using cables is that ability to use a more compact robot architecture that is closer to the biological bipedal walkers. A biological hip joint is a spherical joint with 3 DOF, which basically combines three revolute joints and certainly would contribute to compactness of the robot architecture as well as reducing the total mass (by eliminating the distance links between the corresponding revolute joints).

It is difficult to actuate a spherical joint via directly mounted motors, which is why spherical joints are not usually found in robotic designs with rotary motors. However, it is highly recommended to use spherical (ball and socket) joints when cables are used, as shown in Figure 1. A role of the gear box with rotary joint mounted motors have the small connecting rods (attached at A_1, A_2, K_1, K_2, H_1, H_2 in the figure); the longer the rods, the larger torque is generated by a certain cable force on the expense of larger cable pulling speed (such that the power remains the same).

The walking robot architecture shown in Figure 1 reflects the aspects of cable actuation. With 6 DOF per leg, the architecture enables cornering walk and mimics a biological biped architecture.

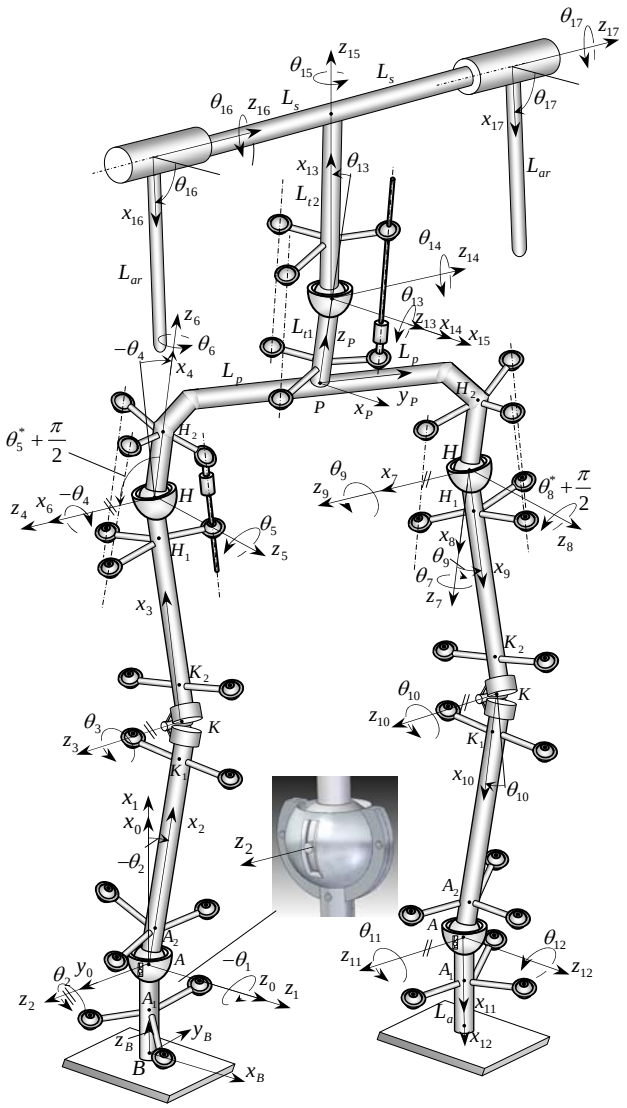

Figure 1. CABLE DRIVEN BIPEDAL WALKING ROBOT ARCHITECTURE

The main purpose of using cables is to relocate the motors that represent the major part of the total robot's weight. The ankle joint is an adjusted spherical joint, with 2 DOF rather than 3DOF, which is

shown in the figure detail. The restriction of one DOF is done by introducing a pin that can slide along the arc shaped guide. The two DOF are the rotation about the axis along the pin, z_2, and the rotation about the axis that is perpendicular to the plane of the arc-shaped guide, z_1.

The ankle joint is actuated via 3 cables and motors that are positioned in the trunk segment of the robot, the segment that experiences much lower accelerations than the ankle position of the leg. This is why there is no purpose to actuate the hip joint via cables, the motors are already near to the low acceleration segment, the trunk. Since the intention is to use the spherical joint for hip, three linear motors are used, each attached between two corresponding smaller ball and socket pairs, as shown in Figure 1.

A difficulty with this concept is that a significant nonlinearity is introduced. While with joint attached motors, the motor shaft rotation is proportional to the rotation about the joint axis, the length of cable pulled is not necessarily proportional to the rotation about the joint axis. This fact becomes particularly important when a controller is designed, which usually requires special treatment either by cancellation of the nonlinearities or by a mathematical model linearization. Another difficulty that accompanies the beneficial features of the cable actuation concept is the possibility of singularities. During the motion, a combination of joint angles might exist such that the direction of cable passes through a joint axis or cables are parallel with a particular axis, which means that the cable cannot generate a moment about that axis (e.g. the singularity can occur at the ankle joint when the three cables are parallel to x_2 axis in Figure 1, or a singularity can occur when the three linear actuators are parallel to z_6 axis of the hip joint).

The nonlinearity between the cable pulling speed and the corresponding joint angular speed can be seen in Figure 2, where a cable actuated knee joint design is shown. The nonlinearity and the difference in the two cable changes require that each cable is pulled independently in case non-stretchable cables are used. If the cable length is increased on one side in the same way as the cable length on the other side of the joint, then one can use a regular pulley with a single motor to actuate the joint. However, this is not the case, very soon from the initial position, one cable would become loose which would cause a pure transport delay in control terms and the walking robot would loose controllability.

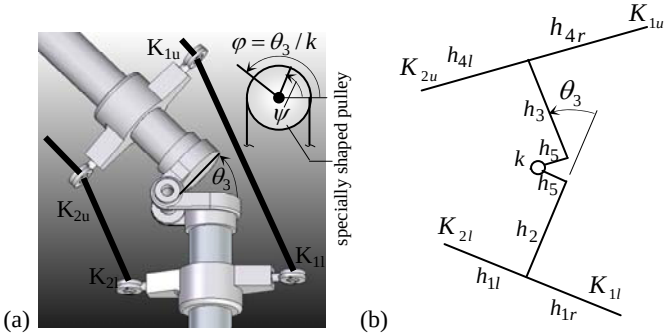

Figure 2. (a) CABLE ATTACHMENT DESIGN, (b) THE CABLE ATTACHMENT POINTS PARAMETERS

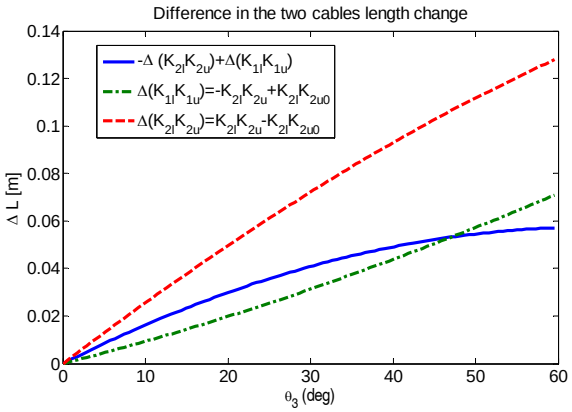

Figure 2. (c) CABLE LENGTH CHANGE DIFFERENCE

The solution to this problem is to design a specially-shaped pulley that will cancel nonlinearities. This pulley profile is shown in Figure 3.

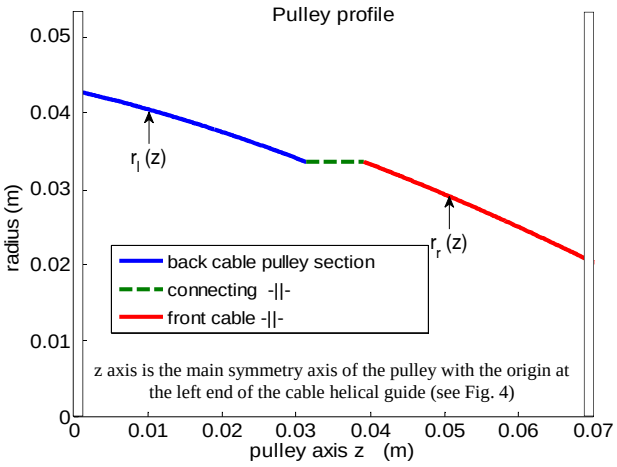

Figure 3. SPECIAL PULLEY PROFILE

The abscissa in the figure denotes the pulley main symmetry axis with the origin on the left hand-side of the helical cable guide, which can be directly proportionally related to the angle of rotation. The cable is stored on the specially shaped pulley in a helical trace, as shown in Figure 4.

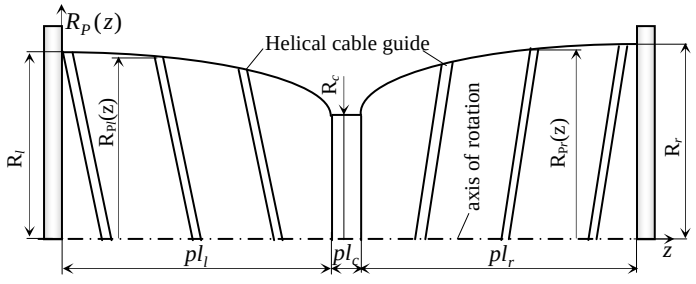

Figure 4. HELICAL CABLE GUIDE

The pulley is attached to a trunk mounted motor and the cables are traced from the trunk to the knee joint. Basically, higher cable pulling

speed at the knee joint means that the cable should be positioned at the larger radius at the pulley, such that no cable become loose. The equation of the pulley profile can be derived by considering how the cable pulling speed is changed while keeping the angular joint rate constant.

$$R_{Pr/l}(\varphi)=\begin{cases} R_{\min}, & \text{for } \pm\dfrac{d\overline{K_{1l}K_{1u}}\ (\theta_3)}{d\theta_3}\Big|_{\theta_3=k\varphi}\left(\dfrac{\delta\theta_3}{\delta\varphi}\right)_{\text{des}} < R_{\min} \\ R_{\max}, & \text{for } \pm\dfrac{d\overline{K_{1l}K_{1u}}\ (\theta_3)}{d\theta_3}\Big|_{\theta_3=k\varphi}\left(\dfrac{\delta\theta_3}{\delta\varphi}\right)_{\text{des}} > R_{\max}, \\ \pm\dfrac{d\overline{K_{1l}K_{1u}}\ (\theta_3)}{d\theta_3}\Big|_{\theta_3=k\varphi}\left(\dfrac{\delta\theta_3}{\delta\varphi}\right), & \text{otherwise.} \end{cases} \quad (1)$$

where $\left(\dfrac{\delta\theta_3}{\delta\varphi}\right)_{\text{des}}=k$ is the desired ratio of the two rotations, $R_{\min}$ is the minimum (positive) radius of the pulley and the derivatives are given in (1), the plus sign is for right hand-side segment of the pulley profile (Figure 3).

Since the machined pulley would always have some error in the profile, in order to prevent a cable becoming loose it is necessary to use stretchable and preloaded cables that will provide some compensation for the inaccuracy in the pulley profile.

On the other hand, since stretchable cables are used, the ratio *k* cannot be precisely constant due to the fact that the cable is stretchable and we cannot compensate the general cable tension force, since it is not only a function of the angles, but also depends on the inertial forces and the payload.

Finally, the architecture (Figure 1) shows that the trunk segment has a spherical joint, which is actuated in a similar fashion as the hip joint, via the three linear actuators. The 3 DOF enable the upper body to deviate from the vertical positions and in that way help to control the position of the Zero Moment Point (ZMP) [16].

3. DYNAMICS OF THE BIPEDAL ROBOT

Using the Lagrange energy method, a set of nonlinear differential equations of second order is derived. Since the derivation details would take significant space, we will include the final results for every particular DOF, but limit the analysis on the sagittal plane, due to the limited space to show details of the transformations between the coordinate systems shown in Figure 1.

The dynamics of the system can be represented by the matrix equation

$$\left[\mathrm{M}(\vec{\theta}(t))\right]\ddot{\vec{\theta}}(t)+\left[\mathrm{C}(\vec{\theta}(t),\dot{\vec{\theta}}(t))\right]\dot{\vec{\theta}}(t)+\vec{\mathrm{P}}(\vec{\theta}(t))=\vec{\tau}(t)\,, \quad (2)$$

where $\vec{\theta}(t)$, $\dot{\vec{\theta}}(t)$ and $\ddot{\vec{\theta}}(t)$ are the joint angle, velocity and acceleration vectors, respectively, $\left[\mathrm{M}(\vec{\theta}(t))\right]$ is the inertial properties matrix, $\left[\mathrm{C}(\vec{\theta}(t),\dot{\vec{\theta}}(t))\right]$ is the angular speed coupling matrix, $\vec{\mathrm{P}}(\vec{\theta}(t))$ is the conservative (generalized) forces vector that includes the gravity terms and cable tension terms and $\vec{\tau}(t)$ is the vector of torques acting at the joints. The product $\left[\mathrm{C}(\vec{\theta}(t),\dot{\vec{\theta}}(t))\right]\dot{\vec{\theta}}(t)$ represents all combined products of the joints angular speed, which is consisted of the Coriolis and relative normal accelerations. Due to limited space, $\left[\mathrm{M}(\vec{\theta})\right]$ and vector $\left[\mathrm{C}(\vec{\theta}(t),\dot{\vec{\theta}}(t))\right]\dot{\vec{\theta}}(t)$ are not shown here.

The vector of the conservative generalized forces $\vec{\mathrm{P}}(\vec{\theta}(t))$ requires an explanation that is related to the further analysis, and we present it below. The vector $\vec{P}(\vec{\theta})$ is

$$\vec{\mathrm{P}}=\begin{bmatrix} m_t g(-l_{t1}s\theta_{234}-l_{t2}c\theta_{234})+m_{2'}g(l_1 s\theta_{2349}+l_{c2'}s\theta_{2349\_10})+m_1 g l_{c1'}s\theta_{2349} \\ \hline k_{sl}\,\Delta l_l(\theta_3,\varphi)\dfrac{-h_{\mathrm{K2s}}c\theta_3-h_{\mathrm{K2c}}s\theta_3}{\overline{K_{2l}K_{2u}}\ (\theta_3)}-m_1 g((l_1-l_{c1})s\theta_{32}-l_{c1'}s\theta_{2349}) \\ +k_{sr}\,\Delta l_r(\theta_3,\varphi)\dfrac{h_{\mathrm{K1s}}c\theta_3-h_{\mathrm{K1c}}s\theta_3}{\overline{K_{1l}K_{1u}}\ (\theta_3)}-m_t g l_{t1}c\theta_{234}+ \\ m_{2'}g(-l_1(s\theta_{32}+s\theta_{2349})-l_{c2'}s\theta_{2349\_10}) \\ \hline m_t g l_{t1}c\theta_{234}+m_1 g((l_1+l_{c1})s\theta_{32}+l_{c1'}s\theta_{2349})+m_{2'}g(l_1(s\theta_{32}+s\theta_{2349}) \\ -l_2 s\theta_3+l_{c2'}s\theta_{2349\_10})-m_2 g l_{c2}s\theta_2 \\ \hline -m_1 g l_{c1'}s\theta_{2349}-m_{2'}g(l_1 s\theta_{2349}+l_{c2'}s\theta_{2349\_10}) \\ \hline k_{sl}\,\Delta l_{lsw}(\theta_{10},\varphi_{\mathrm{sw}})\dfrac{-h_{\mathrm{K2s}}c\theta_{10}-h_{\mathrm{K2c}}s\theta_{10}}{\overline{K_{2l}K_{2u}}\ (\theta_{10})}+ \\ k_{sr}\,\Delta l_{rsw}(\theta_{10},\varphi_{\mathrm{sw}})\dfrac{h_{\mathrm{K1s}}c\theta_{10}-h_{\mathrm{K1c}}s\theta_{10}}{\overline{K_{1l}K_{1u}}\ (\theta_{10})}+m_{2'}g l_{c2'}s\theta_{2349\_10} \end{bmatrix}, \quad (3)$$

where: k_{Sr}, k_{Sl} are the cable stiffness coefficients for the front and the back knee joint cable, respectively,

$$\Delta l_r=\Delta l_r(\theta_3,\varphi)=\overline{K_{1l}K_{1u}}(\theta_3)-\overline{K_{1l}K_{1u\,0}}+\frac{S_{r0}}{k_{Sr}}-\int_0^{\varphi}R_{\mathrm{Pr}}(\psi)\,d\psi\,,\ \text{and}$$

$$\Delta l_l=\Delta l_l(\theta_3,\varphi)=\overline{K_{2l}K_{2u}}(\theta_3)-\overline{K_{2l}K_{2u\,0}}+\frac{S_{l0}}{k_{Sl}}-\int_0^{\varphi}R_{Pl}(\psi)\,d\psi\,, \quad (4)$$

are the deformation of cable springs (in geometrical terms as functions of the knee and the pulley angles (see Figure 2(a)), while the expressions for the spring deformations for the swing leg, Δl_{rsw} and Δl_{lsw}, are analogous to (4) (the deformations are related to external load through algebraic equations of moment balance, by neglecting the pulley dynamics),

- m_1, m_2 and m_t are masses of lower leg, thigh and the trunk, respectively,
- l_1 and l_2 are lower and upper leg lengths, respectively,

- l_{c1} and l_{c2} are distances from the neighboring lower joint to the center of gravity (cg) of lower and upper leg, respectively, and $l_{c1'} = l_1 - l_{c1}$, $l_{c2'} = l_2 - l_{c2}$,
- l_{t1} and l_{t2} denote the position (in the sagittal plane) of the trunk cg with respect to the hip joint lateral axis,
- combined angles are denoted as: $\theta_{32} = \theta_3 - \theta_2$, $\theta_{234} = \theta_2 - \theta_3 + \theta_4$, $\theta_{2349} = \theta_2 - \theta_3 + \theta_4 - \theta_9$, $\theta_{2349\_10} = \theta_2 - \theta_3 + \theta_4 - \theta_9 + \theta_{10}$,
- $h_{K1s} = h_{1r}h_3 + h_2h_{4r}$, $h_{K1c} = -h_2h_3 + h_{1r}h_{4r}$, $h_{K2s} = h_{1l}h_3 + h_2h_{4l}$, $h_{K2c} = -h_2h_3 + h_{1l}h_{4l}$,
- $\overline{K_{1l}K_{1u}} = h_{K1} + h_{K1s}s\theta_3 + h_{K1c}c\theta_3$, $\overline{K_{2l}K_{2u}} = h_{K2} + h_{K2s}s\theta_3 + h_{K2c}c\theta_3$.

The new quantities included in (4) denote the following: S_{r0} and S_{l0} are the cables pre-tensions, $R_{Pr}(\psi)$ and $R_{Pl}(\psi)$ are the two pulley variable radii given by (1) and ψ is the geometrical angle of the cable guide on the pulley, shown in Figure 2. The integrals in (4) represent the stored cable along the pulley thread.

The vector of the torques $\vec{\tau}$ in (2) is

$$\vec{\tau}(t) = \begin{bmatrix} \tau_{\mathrm{h}}(t) & 0 & \tau_{\mathrm{a}}(t) & \tau_{\mathrm{hsw}}(t) & 0 \end{bmatrix}^T, \tag{5}$$

where $\tau_{\mathrm{h}}(t)$ and $\tau_{\mathrm{a}}(t)$ are the torques at the hip and the ankle joints of the stance leg, respectively; $\tau_{\mathrm{hsw}}(t)$ is the torque at the hip of the swing leg. The knee torques are considered here as internal torques, which is why the vector of torques has zeros at the corresponding entries. The two torques are considered in the equations of motion through the spring deformations in the vector (of conservative generalized forces) $\vec{P}$, given by (3).

If we consider the dynamics of the pulleys with the motors, we would have two additional degrees of freedom, as well as two additional differential equations of the second order, which would significantly increase computational efforts without contributing significantly to the accuracy of the mathematical model (inertial and/or viscous friction effects of the drive system are negligible).

The inclusion of the corresponding differential equations into a state space model of the system can be avoided by considering that the pulley/motor dynamics happens instantaneously, which results in an algebraic equation rather than a differential equation. Essentially, the algebraic equations to complete the system of equations are the moment balance equations for the pulley/motor systems (located at the trunk), that is

$$\begin{aligned} &-k_{\mathrm{Sr}}\Delta l_r(\theta_3, \varphi_{st})R_{\mathrm{Pr}}(\varphi_{st}) + k_{\mathrm{Sl}}\Delta l_l(\theta_3, \varphi_{st})R_{Pl}(\varphi_{st}) = \tau_{\mathrm{p}}(t), \\ &-k_{\mathrm{Sr}}\Delta l_r(\theta_{10}, \varphi_{sw})R_{\mathrm{Pr}}(\varphi_{sw}) + k_{\mathrm{Sl}}\Delta l_l(\theta_{10}, \varphi_{sw})R_{Pl}(\varphi_{sw}) = \tau_{\mathrm{psw}}(t), \end{aligned} \tag{6}$$

where τ_p and τ_{psw} are the torques applied on the specially shaped pulleys, R_{Pl} and R_{Pr} are the radii functions of the left and right segment of the pulley, respectively, as shown in Figure 4. The mathematical model (2) along with the two algebraic equations (6) is inherently implicit with the respect to the torque inputs (the vector $\vec{\tau}$ in (5) does not include the pulley torques).

4. CONTROLLER DESIGN

The controller design for the robotic walker is based on the trajectory regulation control [17]. Since the controller algorithm requires the mathematical model of the system be in an affine form, $\dot{\vec{x}} = f(\vec{x}) + [G(\vec{x})]\vec{\tau}$, the dynamics model is made explicit with respect to control inputs (torques), using the algebraic equations (6) and the definition of the pulley radius functions R_P, given by (1). The resulting model in the affine form, required by the control technique, has the vector of torques

$$\vec{\tau}(t) = \begin{bmatrix} \tau_{\mathrm{h}}(t) & \tau_p(t) & \tau_{\mathrm{a}}(t) & \tau_{\mathrm{hsw}}(t) & \tau_{psw}(t) \end{bmatrix}^T, \tag{7}$$

which represents the control inputs vector, while the adjusted vector $\vec{P}(\vec{\theta}(t))$ does not have the terms with cable stiffness parameter. After expressing the model in the affine form, the trajectory regulation control technique can be applied.

4.1 Controller Architecture

The control system architecture (Figure 5) consists of [17]:

(a) Nominal trajectories generator,
(b) Inverse dynamics for nominal control calculation,
(c) Tracking error regulation controller,
(d) Measurement system, and
(e) Plant – the biped.

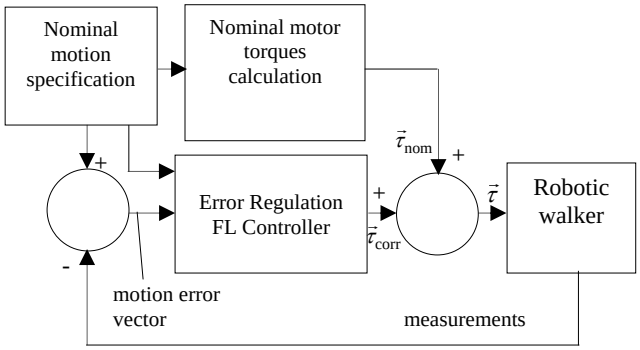

Figure 5. THE TRAJECTORY REGULATION CONTROLLER ARCHITECTURE

The nominal motion specification block generates the joint trajectories that provide a balanced walk. The information about the nominal joint angles at every time-step is sent to the error dynamics controller and the nominal torques generator. The nominal torques are generated based on the inverse dynamics mathematical model. Since the mathematical model of the robot is not an exact description of the dynamic behavior, there will be errors in the resulting motion. The amount of the resulting motion deviation from the desired motion is

calculated based on the measurements of the joint's angles, which is used by the error dynamics controller to generate the correction torques.

The inverse dynamics that is used to generate the nominal torques is obtained directly from (2), where the torques are explicitly expressed in terms of the functions of angles and their first two derivatives. However, physically realizable approximations of input signals derivative are obtained via a second order low-pass filter of the form (in the Laplace domain)

$$\Phi(s)=\frac{s}{\varepsilon_1 s^2+\varepsilon_2 s+1},\quad \varepsilon_{1,2}\in\left[10^{-3},10^{-2}\right].$$

Since the controller architecture is based on the error dynamics, we need to obtain the corresponding error dynamics model.

4.2 Error dynamics

The error dynamics model is based on the state space model in affine form and it has the following form

$$\begin{bmatrix}\dot{\tilde{\xi}}_1\\ \dot{\tilde{\xi}}_2\\ \dot{\tilde{\xi}}_3\\ \dot{\tilde{\xi}}_4\\ \dot{\tilde{\xi}}_5\\ \dot{\tilde{\xi}}_6\\ \dot{\tilde{\xi}}_7\\ \dot{\tilde{\xi}}_8\\ \dot{\tilde{\xi}}_9\\ \dot{\tilde{\xi}}_{10}\end{bmatrix}=\begin{bmatrix}\tilde{\xi}_2\\ f_2(\vec{\xi})-f_2(\vec{\bar{\xi}})\\ \tilde{\xi}_4\\ f_4(\vec{\xi})-f_4(\vec{\bar{\xi}})\\ \tilde{\xi}_6\\ f_6(\vec{\xi})-f_6(\vec{\bar{\xi}})\\ \tilde{\xi}_8\\ f_8(\vec{\xi})-f_8(\vec{\bar{\xi}})\\ \tilde{\xi}_{10}\\ f_{10}(\vec{\xi})-f_{10}(\vec{\bar{\xi}})\end{bmatrix}+\begin{bmatrix}0 & 0 & \cdots & 0\\ G_{11}(\vec{\bar{\xi}}) & G_{12}(\vec{\bar{\xi}}) & \cdots & G_{15}(\vec{\bar{\xi}})\\ 0 & 0 & \cdots & 0\\ G_{21}(\vec{\bar{\xi}}) & G_{22}(\vec{\bar{\xi}}) & \cdots & G_{25}(\vec{\bar{\xi}})\\ 0 & 0 & \cdots & 0\\ G_{31}(\vec{\bar{\xi}}) & G_{32}(\vec{\bar{\xi}}) & \cdots & G_{35}(\vec{\bar{\xi}})\\ 0 & 0 & \cdots & 0\\ G_{41}(\vec{\bar{\xi}}) & G_{42}(\vec{\bar{\xi}}) & \cdots & G_{45}(\vec{\bar{\xi}})\\ 0 & 0 & \cdots & 0\\ G_{51}(\vec{\bar{\xi}}) & G_{52}(\vec{\bar{\xi}}) & \cdots & G_{55}(\vec{\bar{\xi}})\end{bmatrix}\begin{bmatrix}\tilde{\tau}_{\mathrm{h}}\\ \tilde{\tau}_{\mathrm{p}}\\ \tilde{\tau}_{\mathrm{a}}\\ \tilde{\tau}_{\mathrm{hsw}}\\ \tilde{\tau}_{\mathrm{psw}}\end{bmatrix},\quad (8)$$

where $\vec{\bar{\xi}}$ denotes the nominal trajectory of the system state (regarding the robot angles and angular velocities) in the state space, $\tilde{\xi}_i=\xi_i-\bar{\xi}_i$ is the error of the i-th variable with respect to its nominal value for the specified time and $\tilde{\tau}_j$ (j ∈ {h,p,a,hsw,psw}) represents corrective torque inputs, generated by the feedback controller with the objective to have the error vector norm $\left\|\vec{\tilde{\xi}}\right\|\to 0$ (exponentially). The way the error vector is stabilized is discussed in the following section.

4.3 Control Law

The control law should provide the corrective torques such that the errors converge to zero with an exponential decay. To achieve this goal the control inputs cancel the nonlinearity (FL technique) and introduce the terms proportional to the errors of the state variables as follows.

$$\begin{aligned}
&G_{11}\tau_h+G_{12}\tau_p+G_{13}\tau_a+G_{14}\tau_{hsw}+G_{15}\tau_{psw}=\tilde{b}_{g1},\\
&G_{21}\tau_h+G_{22}\tau_p+G_{23}\tau_a+G_{24}\tau_{hsw}+G_{25}\tau_{psw}=\tilde{b}_{g2},\\
&G_{31}\tau_h+G_{32}\tau_p+G_{33}\tau_a+G_{34}\tau_{hsw}+G_{35}\tau_{psw}=\tilde{b}_{g3},\quad (9)\\
&G_{41}\tau_h+G_{42}\tau_p+G_{43}\tau_a+G_{44}\tau_{hsw}+G_{45}\tau_{psw}=\tilde{b}_{g4},\\
&G_{51}\tau_h+G_{52}\tau_p+G_{53}\tau_a+G_{54}\tau_{hsw}+G_{55}\tau_{psw}=\tilde{b}_{g5},
\end{aligned}$$

where

$$\begin{aligned}
\tilde{b}_{g1}&=-f_2(\vec{\xi})+f_2(\vec{\bar{\xi}})-k_{21}\tilde{\xi}_1-k_{22}\tilde{\xi}_2,\\
\tilde{b}_{g2}&=-f_4(\vec{\xi})+f_4(\vec{\bar{\xi}})-k_{43}\tilde{\xi}_3-k_{44}\tilde{\xi}_4,\\
\tilde{b}_{g3}&=-f_6(\vec{\xi})+f_6(\vec{\bar{\xi}})-k_{65}\tilde{\xi}_5-k_{66}\tilde{\xi}_6,\\
\tilde{b}_{g4}&=-f_8(\vec{\xi})+f_8(\vec{\bar{\xi}})-k_{87}\tilde{\xi}_7-k_{88}\tilde{\xi}_8,\\
\tilde{b}_{g5}&=-f_{10}(\vec{\xi})+f_{10}(\vec{\bar{\xi}})-k_{109}\tilde{\xi}_9-k_{1010}\tilde{\xi}_{10},
\end{aligned}$$

and k_{ij} (i=2,4,...,10; j=i-1,i) are the constants that need to be determined, such that the closed control loop error dynamics are exponentially stable and have desired transient behavior.

Particularly, we can set up the constraint that the system has less than 5% overshoot, and the settling time less than 0.5 seconds for each joint rotational DOF, which results in the damping coefficient $\zeta>0.69$ and the natural frequency $\omega_{\mathrm{n}}>11.59\frac{\mathrm{rad}}{\mathrm{s}}$. To obtain the two values, the coefficients k_{ij} need to have the following values

$$k_{i,i-1}=134.3\ \left(\frac{\mathrm{rad}}{\mathrm{s}}\right)^2,\ k_{ii}=16\ \left(\frac{\mathrm{rad}}{\mathrm{s}}\right),\ (i=2,4,...,10).$$

Finally, the control law is

$$\vec{\tilde{\tau}}=G^{-1}\vec{\tilde{b}}_g,\quad (10)$$

Where G is the reduced input matrix in (8) (without zero rows) evaluated at the nominal trajectory $\vec{\bar{\xi}}$. Next, we will evaluate the performance of the control law via simulation results.

4.4 Nominal Joint Trajectories

Nominal trajectories should be designed such that the bipedal robot has a balanced walk and that the controller has relatively low corrections (within the area of attraction AOA). Basic tool for calculating the trajectories toward this goal is the Zero Moment Point (ZMP) calculation. Biped needs to keep ZMP within the convex region defined by the feet prints on the ground in order to have a balanced walk. Figure 6 shows the nominal ZMP trajectory, which is designed such that: (i) it passes through the middle points of foot prints, (ii) it is confined within the convex hull (enclosed by the dashed line in Figure 6) and (iii) the tangent line at those points is parallel to x_{B} axis (the coordinate system is shown in Figure 1).

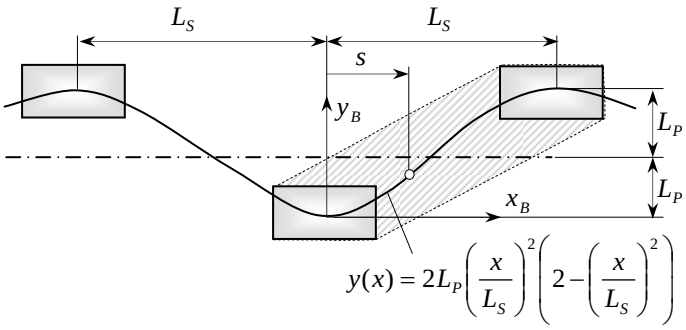

Figure 6. ZERO MOMENT POINT TRAJECTORY

The trajectory function

$$y(x) = 2L_P\left(\frac{x}{L_S}\right)^2\left(2-\left(\frac{x}{L_S}\right)^2\right),\ -L_S \le x \le L_S \qquad (11)$$

is obtained via interpolation with the slope constraints. Whole dynamics (gravitational and inertial forces) of the system influences the position of the ZMP (center of pressure for a balanced walk). For a relatively slow walk, the ZMP is close to the COM ground projection and calculation is significantly simplified.

On the other hand, we can design the trajectory of the center of mass in the vertical plane such that it follows a trajectory of a simplified model that is used of an energy optimization, like a mass and spring model, as shown in Figure 7.

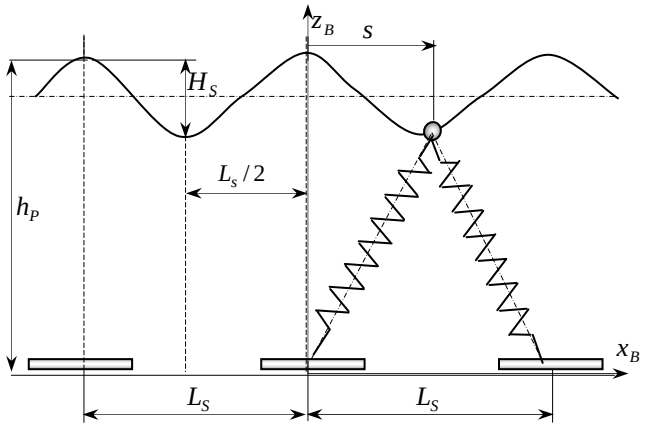

Figure 7. CENTER OF MASS TRAJECTORY

An energy optimized trajectory obtained by simple models (mass-spring) is, of course, not energy optimized for the higher complexity model, like the one shown in Figure 1, but it provides a way of energy reduction. Particularly, in this case the following trajectory was used:

$$z(x) = H_P + H_S\left(\frac{x}{L_S/2}\right)^2\left(-2+\left(\frac{x}{L_S/2}\right)^2\right), \qquad (12)$$

which in a dimensionless form is

$$\zeta(\xi) = \frac{H_P}{H_S/2}2\xi^2\left(-2+\xi^2\right),\ \xi = \frac{x}{L_S/2},\ \zeta = \frac{z(x)}{H_S/2},$$

with the domain $-1 \le \xi \le 1$.

Using this approach the joint trajectories for the stance leg are obtained, as shown in Figure 8.

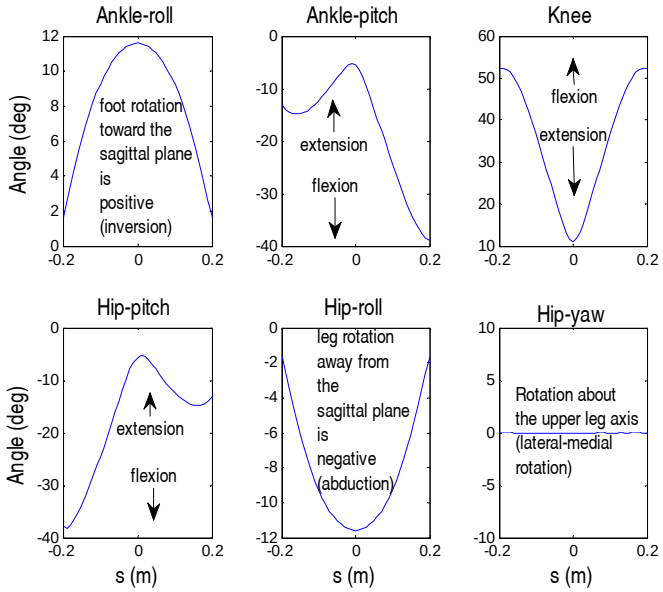

Figure 8. NOMINAL JOINT TRAJECTORIES

Using the nominal joint trajectories and kinematic analysis of the system, the cable pulling speed is calculated. In a similar way, by considering the distance between the cable attachment points as a function of joints angles and by finding the corresponding vectors in directions of the cable segments, three-dimensional vectors of the moments and the cable forces are calculated and shown in the following figures. The stance leg knee joint cable force magnitudes are shown in Figure 9.

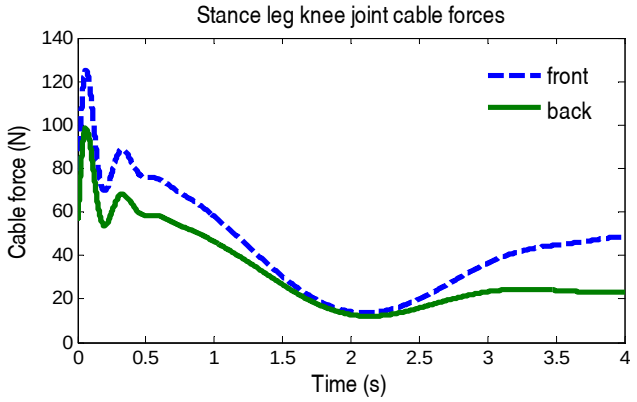

Figure 9. STANCE LEG KNEE JOINT CABLE FORCES

Simulations of the system showed that the way the cables are attached, particularly the position of the attaching rods at the points A_1, A_2, K_1, K_2, H_1, H_2 (Figure 1), has a dominant influence on the required cable forces and required cable speed.

The ankle joint cable forces are shown in Figure 10. The cable forces for the ankle joint are significantly higher than for the knee joint.

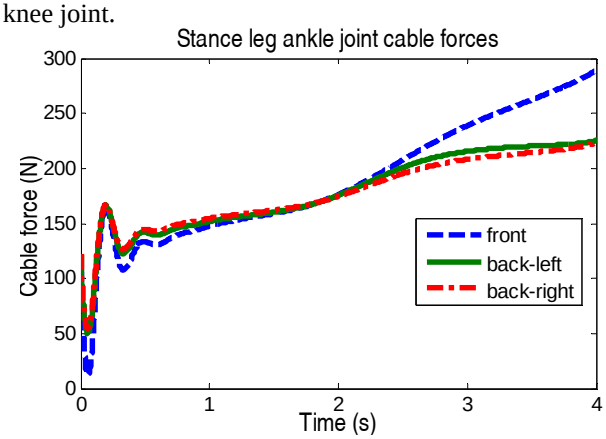

Figure 10. STANCE LEG ANKLE JOINT CABLE FORCES

The cable actuators act in some way as parallel manipulators and form closed mechanical loops. Unlikely with serial robotic manipulators, there can be infinitely many solutions for the set of cable forces providing the same torque for the joint. In this case, it is useful to use an optimization approach and derive additional constraints which will choose the solution among infinitely many providing the same joint moment. An additional criterion, for example, can be to minimize a sum of squares of cable tensions, but considering the inherited constraint that cables can deliver only tension forces.

Unlike the cable forces for the knee and the ankle joints, the linear actuator forces for the hip joint can deliver tension and compression forces as well, which is why three actuators are sufficient for the spherical joint (3 DOF), rather than four which would be needed in the case of using cables (number of cables needed for an n DOF joint is n+1, so it would be 4 for the hip joint).

The linear actuator forces for the stance leg hip joint are shown in Figure 11. The calculation of the forces included the pitch and the roll moment, as well.

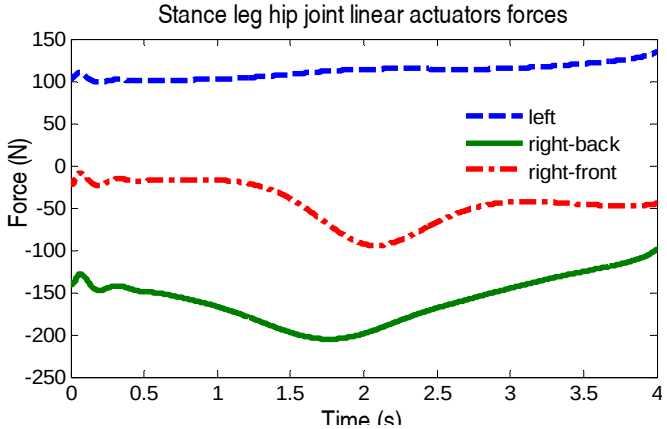

Figure 11. STANCE LEG HIP JOINT LINEAR ACTUATOR FORCES

The realized angles of the stance and swing leg, without rolling at the hip and the ankle, are compared with the nominal trajectories in Figure 12. Although the pitch angles at the hip and the ankle are negative, according to the definitions shown in Figure 1, they are represented in the following figures with the same sign, in other to better use the space available for comparison. Figure 12 shows good performance of the controller since the trajectories are followed closely with minor errors. It is necessary to emphasize that the trajectories shown in the figure are obtained for a stationary (non-accelerating) walk, such that the joint trajectories show the cyclic behavior and symmetry.

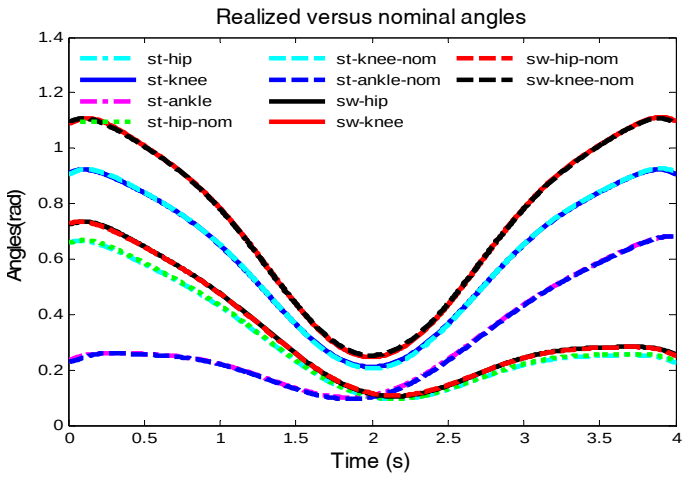

Figure 12. REALIZED VERSUS NOMINAL JOINT TRAJECTORIES

When the system starts from the rest, the nominal trajectories at the initial instant behave like step functions, requesting the joints to "suddenly" change angles according to the initial conditions. In this situation, the controller shows a bit worse performance, but it guides the system toward the stationary walking cycle without loosing the stability, as shown in Figure 13.

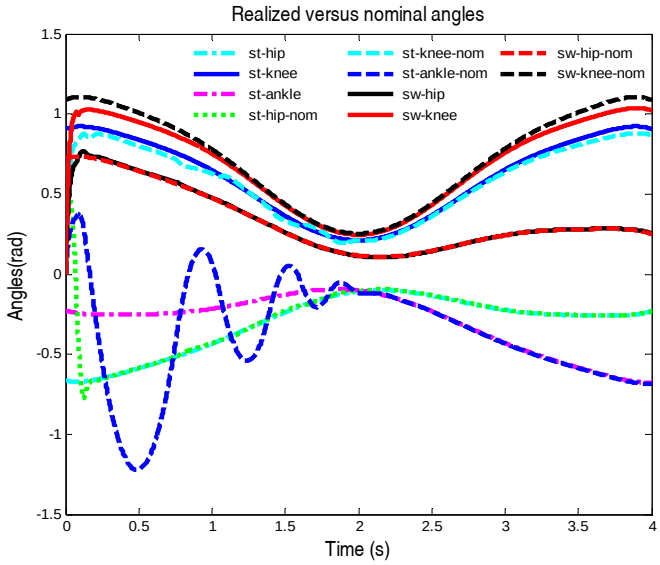

Figure 13. CONTROLLER PERFORMANCE: REALIZED VERSUS NOMINAL ANGLES FOR AN UNSTEADY WALK PHASE

In this case, all trajectories start from the origin and the highest oscillation happens at the stance leg ankle joint, as expected due to the fact that the highest forces/torques are needed at the ankle joint.

The total (nominal plus correction) torques related to the sagittal plane motion for the stance and the swing leg are shown in Figure 14.

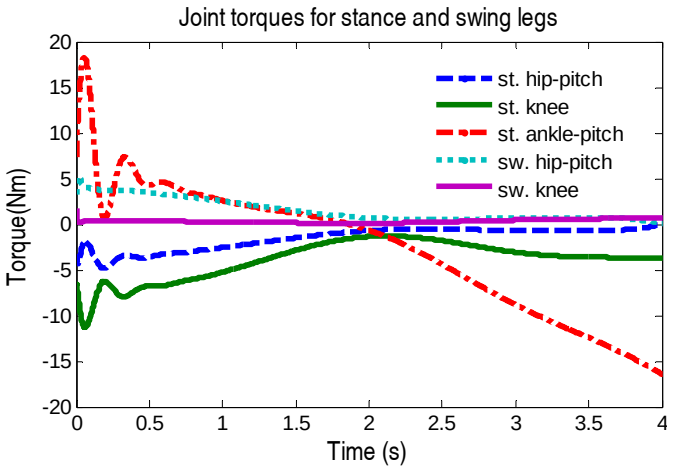

Figure 14. STANCE AND SWING LEG TOTAL TORQUES

It can be noticed that the lowest values for the torques are associated to the joints on the swing leg, due to the fact that those joints do not "see" the trunk weight or the trunk inertial forces as their load.

The corrective torques generated by the error regulation controller are shown in Figure 15, with a peek value of 12 Nm in the initial phase of the cycle.

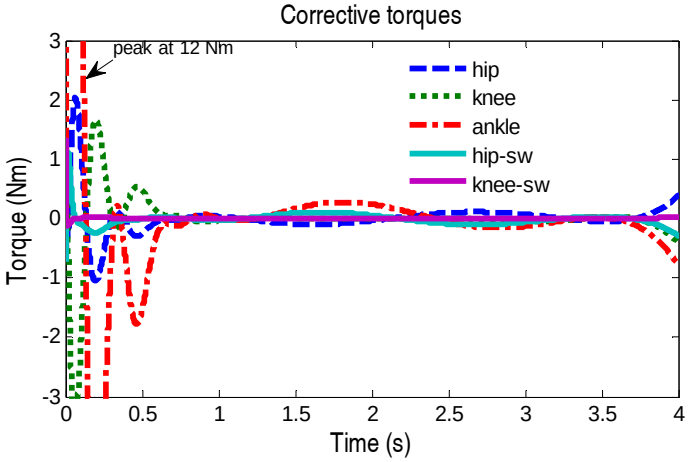

Figure 15. STANCE AND SWING LEG CORRECTIVE TORQUES

The nominal torques obtained by the inverse system (inverse plant) are shown in Figure 16. Those are the torques that would, in an ideal case of knowing exact dynamics of the system, drive the system exactly according to the nominal trajectories, which is not the case in real application and an error regulation/ tracking controller is necessary to combine with the inverse plant. In absence of the inverse plant, the controller would need some additional time such that the integrators find the nominal values.

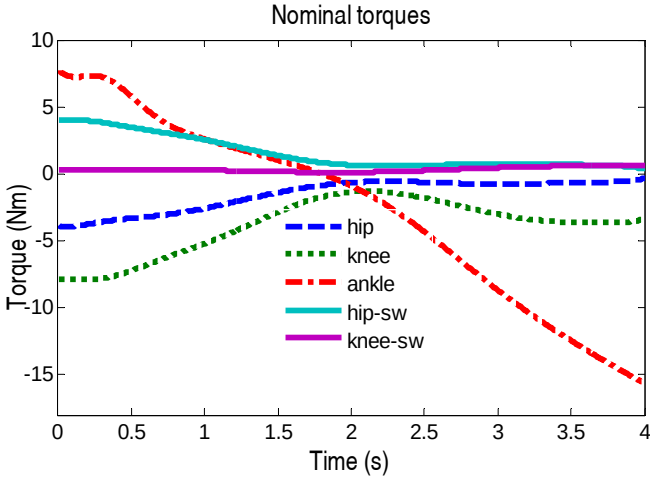

Figure 16. STANCE AND SWING LEG NOMINAL TORQUES

The inverse plant generates the nominal torques based on the derivatives of the nominal joint trajectories, shown in Figure 17. Calculating of the derivatives is done via pseudo-differentiators (filters) of second order. Pseudo-differentiators help to reduce the effect of eventual discontinuities, sharp slope changes or a noise in the input trajectories signals. All derivatives start from the origin (zero), due to the fact that the derivatives are obtained as outputs from a second order system (the filter). However, outputs find the corresponding values for the derivatives relatively fast.

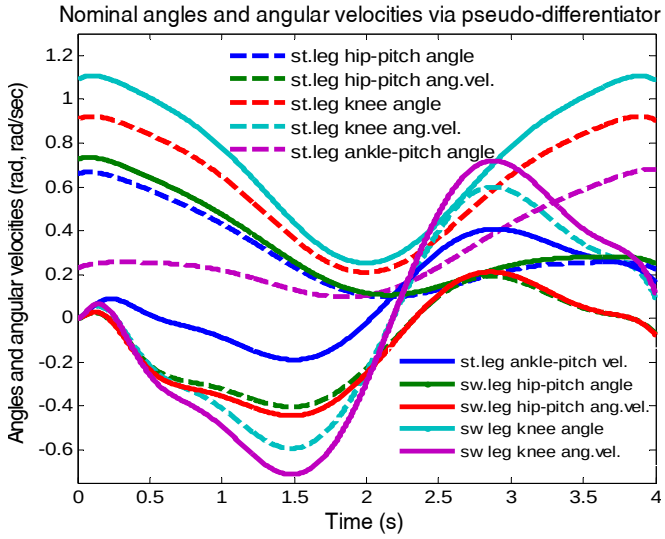

Figure 17. STANCE AND SWING LEG NOMINAL ANGLES AND ANGULAR VELOCITIES OBTAINED USING PSEUDODIFFERENTIATORS

CONCLUSION AND FUTURE WORK

The article presented a novel approach of an actuation system design for bipedal robotic walkers, the design that uses elastic cables. This concept enables a compact robotic architecture biologically inspired due to the fact that biological walkers are considered much closer to the optimality in terms of energy expenditure. The fact that the

major part of the robot weight corresponds to actuators makes the concept how the actuators are positioned very important for two main reasons:

(i) Joint mounted motors positioned on the most kinetically active robot links, such as the lower leg, experience high inertial forces, meaning that other actuators of the robot "see" the particular motor as an additional weight – load that need to be carried, accelerated/decelerated frequently during every step.

(ii) Besides the fact that frequent acceleration and deceleration costs significant amount of energy, it impedes the balancing capabilities of bipedal walkers due to the additional inertial forces acting as a disturbance to the controller.

The need of using two different pulley-motor pairs to actuate a revolute joint in case of using non-stretchable cables is compensated using the stretchable cables with the design of the special pulley profile. The threaded pulley profile with the variable radius ensured that, along with relatively small deformations of the cable spring, the cables do not become loose, which would lead directly into complications with "pure transport delays" in the control law.

A potential problem of using elastic cables can be high amplitude oscillations in the case if there is no sufficient attenuation in the system (friction). In this case, the controller has to be capable of stabilizing the walk, which can be an accompanying challenge of the controller design.

The mathematical model is derived and the corresponding error dynamics is used to design the controller using the trajectory regulation control with an open-loop nominal controller and a closed loop tracking error regulation controller. The nominal controller is based on the inverse dynamics model of the plant. The closed-loop controller is based on the feedback linearization control, where plant nonlinearity is cancelled by state feedback, and desired linear dynamics properties are assigned (eigenvalues).

The performance of the joint trajectories tracking was analyzed using simulations, which showed satisfactory results of tracking the prescribed joint trajectories. The possible problematic cases of the tracking would be the cases with the sharp changes and/or associated noise in the desired trajectories, due to the need of finding (approximate) derivatives. The controller performed satisfactorily by tracking nominal trajectories under relatively high initial disturbance due to significant discontinuity in the commanded trajectories.

Our future work plan mainly consists of implementing the design and proving the concept in hardware. A quadruped walking robot, partially cable actuated with the specially shaped pulleys has been built, which can be seen at:

www.youtube.com/watch?v=sZZpKn_nDIc
www.youtube.com/watch?v=ZCydQB9Vyfo

Radio-controlled servomotors are used with a built in (local loop) angular position controller. Currently the RoboCat employs a statically stable walking gait, with standard Radio Controlled (R/C) servo motors as actuators. The joint motion control scheme is open-loop in nature, which limits the robot's performance in sense of walk smoothness.

We plan to implement this concept and build a bipedal walking robot.

REFERENCES

[1] world.honda.com/ASIMO/
[2] www.takanishi.mech.waseda.ac.jp/top/research/wabian
[3] Giovanni A. Cavagna, Norman C. Heglund, and C. Richard Taylor, Mechanical work in terrestrial locomotion: two basic mechanisms for minimizing energy expenditure. *Am J Physiol.*; **233,** 1977.
[4] Brian R. Umberger and Philip E. Martin, "Mechanical power and efficiency of level walking with different stride rates", *The Journal of Experimental Biology*, **210**, pp. 3255-326, 2007.
[5] Ruina, A., Bertram, J. E., & Srinivasan, M., A collisional model of the energetic cost of support work qualitatively explains leg sequencing in walking and galloping, pseudo-elastic leg behavior in running and the walk-to-run transition. *Journal of Theoretical Biology*, **237**, pp. 170–192, 2005.
[6] Vanderborght Bram, Van Ham Ronald, Verrelst Bjorn, Van Damme Michael, Lefeber Dirk, "Overview of the Lucy Project: Dynamic Stabilization of a Biped Powered by Pneumatic Artificial Muscles," *Advanced Robotics*, **22**, pp. 1027–1051, 2008.
[7] Hirai, K., Hirose, M., and Takenaka, T., 1998, "The Development of Honda Humanoid Robot," *IEEE International Conference on Robotics & Automation*, Leuven, Belgium, Vol. 1, pp. 1321-1326.
[8] Hobbelen, D., Boer,. T., and Wisse, M., 2008, "System overview of bipedal robots Flame and TUlip: tailor-made for Limit Cycle Walking," *IEEE/RSJ International Conference on Intelligent Robots and Systems*, Nice, France, pp. 2486- 2491.
[9] Vanderborght Bram, Van Ham Ronald, Verrelst Bjorn, Van Damme Michael, Lefeber Dirk, "Overview of the Lucy Project: Dynamic Stabilization of a Biped Powered by Pneumatic Artificial Muscles," *Advanced Robotics*, **22**, pp. 1027–1051, 2008.
[10] Ray H. Baughman, "Playing Nature's Game with Artificial Muscles," *Science*, **308**, pp. 63-65, 2005.
[11] Yoseph Bar-Cohen and Sean Leary, "Electroactive Polymers as Artificial Muscles changing Robotics Paradigms," National Space and Missile Materials Symposium, 2000.
[12] Ali E. Aliev et al., "Giant-Stroke, Superelastic Carbon Nanotube Aerogel Muscles," *Science*, **323**, pp. 1575-1578, 2009.
[13] E. Kljuno and R.L. Williams II, "Vehicle Simulation System: Controls and Virtual-Reality-Based Dynamics Simulation", *Journal of Intelligent and Robotic Systems*, **52**, pp. 79-99, 2008.
[14] Alan P. Bowling, "Mass Distribution Effects on Dynamic Performance of a Cable-Driven Hexapod," *ASME Journal of Mechanical Design*, vol. 129, no. 8, pp. 887-890, 2007.
[15] Elvedin Kljuno, Jim J. Zhu, Robert L. Williams II and Stephen M. Reilly, "A Biomimetic Elastic Cable Driven Quadruped Walking Robot – RoboCat," *ASME*, IMECE, 2011.
[16] Vukobratovic, M., and Juricic, D., 1969, "Contribution to the Synthesis of Biped Gait", IEEE Trans. on Bio-Medical Engineering, BME-16, No.1, pp. 1-6.
[17] Khalil, H. K., "Nonlinear Systems," 2nd Edition, Englewood Cliffs, NJ, Prentice-Hall, 1996.